PCCP

PAPER

View Article Online
View Journal | View Issue

Cite this: *Phys. Chem. Chem. Phys.*, 2018, **20**, 11692

Dissociative electron attachment and electronic excitation in $Fe(CO)_5$†

M. Allan,*[a] M. Lacko,[b] P. Papp,[b] Š. Matejčík,[b] M. Zlatar,[c] I. I. Fabrikant,[d] J. Kočišek[e] and J. Fedor*[e]

Received 2nd March 2018,
Accepted 27th March 2018

DOI: 10.1039/c8cp01387j

rsc.li/pccp

In a combined experimental and theoretical study we characterize dissociative electron attachment (DEA) to, and electronically excited states of, $Fe(CO)_5$. Both are relevant for electron-induced degradation of $Fe(CO)_5$. The strongest DEA channel is cleavage of one metal–ligand bond that leads to production of $Fe(CO)_4^-$. High-resolution spectra of $Fe(CO)_4^-$ reveal fine structures at the onset of vibrational excitation channels. Effective range R-matrix theory successfully reproduces these structures as well as the dramatic rise of the cross section at very low energies and reveals that virtual state scattering dominates low-energy DEA in $Fe(CO)_5$ and that intramolecular vibrational redistribution (IVR) plays an essential role. The virtual state hypothesis receives further experimental support from the rapid rise of the elastic cross section at very low energies and intense threshold peaks in vibrational excitation cross sections. The IVR hypothesis is confirmed by our measurements of kinetic energy distributions of the fragment ions, which are narrow (~0.06 eV) and peak at low energies (~0.025 eV), indicating substantial vibrational excitation in the $Fe(CO)_4^-$ fragment. Rapid IVR is also revealed by the yield of thermal electrons, observed in two-dimensional (2D) electron energy loss spectroscopy. We further measured mass-resolved DEA spectra at higher energies, up to 12 eV, and compared the bands observed there to resonances revealed by the spectra of vibrational excitation cross sections. Dipole-allowed and dipole/spin forbidden electronic transitions in $Fe(CO)_5$—relevant for neutral dissociation by electron impact—are probed using electron energy loss spectroscopy and time-dependent density functional theory calculations. Very good agreement between theory and experiment is obtained, permitting assignment of the observed bands.

1 Introduction

Iron pentacarbonyl, $Fe(CO)_5$, has been traditionally used as a precursor for chemical vapor deposition (CVD). Recent advances in nanofabrication technology promise a novel use of it as a precursor in focused electron-beam induced deposition (FEBID). FEBID is a direct-write technique for producing spatially well-defined nanostructures by locally dissociating the metal-containing precursor molecules with a focused electron beam that strips off the ligands and leaves ideally a pure metal behind. A variety of metals can be deposited this way.[1] The possibility of creating controlled high-purity structures of iron attracts special attention due to their magnetic properties, promising use in nanosensing applications. $Fe(CO)_5$ is the most commonly used precursor for FEBID deposition of iron[1] and several reports on its use have been published.[2–4]

The electron beam in FEBID has energies of many kilo-electronvolts that allow its nm-sized focusing. Unfortunately, the deposits themselves are usually much broader than the primary beam. This appears to be due to the decomposition of a large fraction of the precursor by interactions with secondary electrons, which are spatially much more spread, and whose energy distribution usually peaks around 10 eV, or even below that.[5] The second common problem is that the purity of the deposits is often low—the interactions with secondary electrons lead to incomplete separation of ligands. A number of purification techniques have been suggested to compensate for this effect—for example reductive reactions by atomic hydrogen[6] or oxidative reactions with electron impact stimulated water,[7] but making a pure

[a] *Department of Chemistry, University of Fribourg, Chemin du Musée 9, 1700 Fribourg, Switzerland. E-mail: michael.allan@bluewin.ch*
[b] *Department of Experimental Physics, Comenius University, Mlynská dolina F2, 84215 Bratislava, Slovakia*
[c] *Department of Chemistry, Institute of Chemistry, Technology and Metallurgy (IChTM), University of Belgrade, Njegoševa 12, P. O. Box 815, 11001 Belgrade, Serbia*
[d] *Department of Physics and Astronomy, University of Nebraska, Lincoln, NE 68588-0299, USA*
[e] *J. Heyrovský Institute of Physical Chemistry v.v.i., Czech Academy of Sciences, Dolejškova 3, 18223 Prague 8, Czech Republic. E-mail: juraj.fedor@jh-inst.cas.cz*

† Electronic supplementary information (ESI) available: Tables with configurations and energies of calculated excited electronic states. See DOI: 10.1039/c8cp01387j

deposit directly would be preferable. For iron pentacarbonyl it has been shown that under specific ultrahigh vacuum conditions the autocatalytic decomposition leads to a purity of up to 95%.[3]

The desire to resolve these problems has sparked interest in the elementary electron-induced dissociative processes in metal-containing precursor molecules including iron pentacarbonyl. An early DEA study was performed by Compton and Stockdale.[8] A more recent DEA spectrum was presented by Schukin *et al.*[9] An early study of thermal electron attachment in an ion cyclotron resonance (ICR) cell was performed by George and Beauchamp.[10] Attachment rates of slow electrons to $Fe(CO)_5$ (and also $Fe(CO)_n$, n = 0–4) were measured using a flowing afterglow Langmuir probe apparatus by Shuman *et al.*[11] A study of processes involving positive ions—complementary to the present investigation—has been performed by Lacko *et al.*[12] A preliminary account of a study involving negative ion intermediates was presented in conference proceedings.[13] Processes induced by electron transfer in Rydberg atom collisions were studied by Buathong *et al.*[14] Related to the present work are also condensed phase studies—electron induced degradation of condensed $Fe(CO)_5$ by electron stimulated desorption has been studied by Massey *et al.*[15,16] and Hauchard and Rowntree[17]—and studies on argon nanoparticles by Lengyel *et al.*[18,19] The electron affinity of $Fe(CO)_4$, required for the interpretation of the present data, was determined by anion photoelectron spectroscopy by Engelking and Lineberger.[20]

Electron-induced decomposition of $Fe(CO)_5$ has so far been probed experimentally with respect to identifying which fragmentation pathways occur, which electron energy ranges are relevant and, in some cases, determining absolute cross sections. However, little is known about the dissociation mechanisms, that is, what resonances serve as doorway states and what are their properties. Experimentally, probing of the mechanisms requires high electron-energy resolution in order to reveal as many details as possible. Theoretically, an advanced treatment is required that is able to describe both electronic states embedded in continuum and bound excited electronic states, both being non-trivial tasks. Here we present a detailed study of the fragmentation mechanisms in iron pentacarbonyl. We focus on two processes—fragmentation by dissociative electron attachment (DEA) and electronic excitation (EE) by electron impact, which is the initial step in neutral dissociation (ND).[21] A high electron energy resolution experiment reveals previously unreported fine features in the DEA spectra and provides information about electron impact-induced electronic excitation. Both experiments are very well reproduced by two different theoretical approaches: effective range theory with complex boundary conditions for DEA and time-dependent density functional theory for the electronic excitation.

2 Experimental methods

Two experimental setups have been used.

The high-resolution DEA and electron-energy loss (EELS) spectra were measured on an electron spectrometer with hemispherical analyzers.[22,23] The energy of the incident beam was calibrated on the 19.365 eV ^2S resonance in helium. Electron-energy resolution was 17 meV and incident electron energies down to 20 meV could be reached. A magnetic angle changer built around the collision region permits measurements in the full angular range, even at the normally inaccessible angles of 0° (forward scattering) and 180° (backward scattering). The analyzer is equipped with a Wien filter placed just before the channeltron and allows for selective detection of electrons or ions, albeit without resolving the individual ion masses.

Spectra resolved with respect to masses of the fragment ions were therefore recorded separately in a crossed electron and molecular beam apparatus with a quadrupole mass filter.[24] The molecular beam in this instrument is formed by effusion of the $Fe(CO)_5$ vapor *via* a small capillary into the vacuum. In the reaction region, molecules collide with an electron beam, generated by a trochoidal electron monochromator. Electron energy resolution of around 200 meV was used in this study and the electron energy scale was calibrated using SF_6 gas, which yields a strong SF_6^- signal at 0 eV. A weak electric field extracts the produced ions from the reaction region into the ion optics of the quadrupole mass analyzer. The mass-separated ions were detected by an electron multiplier.

3 Theoretical methods

3.1 Effective range theory with complex boundary conditions

The treatment follows the lines applied previously to SF_6 by Fabrikant and coworkers[25,26] and the early qualitative concepts presented by Gauyacq and Herzenberg.[27] The challenge lies in properly describing the effects of the long-range electron–molecule interaction. If sufficiently strong, it will support a weakly bound (diffuse) anion state. However, even if the interaction is not strong enough to support such dipole-bound state, but only slightly weaker, it will strongly influence the low-energy scattering. The incident electron feels the interaction potential and, in terms of the scattering theory, a virtual ('slightly unbound') state can be formed.[28]

We assume that at the first stage the incoming *s*-wave electron distorts the nuclear framework by coupling to a symmetric CO stretch motion with simultaneous capture. The energy deposited by the electron is then distributed by intramolecular vibrational redistribution (IVR) over all the nuclei in a chaotic longer-lived anion state. This energy is channeled eventually either into breaking the Fe–CO bond and 'evaporation' of the CO fragment, or into electron detachment. The electronic part of the problem, the electron capture and excitation of the symmetric stretch mode, is described by the effective range theory (ERT) which has demonstrated its capacity to describe the subtleties of extremely short-lived anion states such as nonlocal effects and the transition region from the virtual state into the bound state. This task is currently far out-of-reach of *ab initio* calculations. IVR is then modeled by complex boundary conditions.

The iron pentacarbonyl molecule has 27 vibrational degrees of freedom and a complete theoretical description of nuclear dynamics is currently not possible. However, already a preliminary glance at the high resolution ion yield spectrum in part (b) of Fig. 1

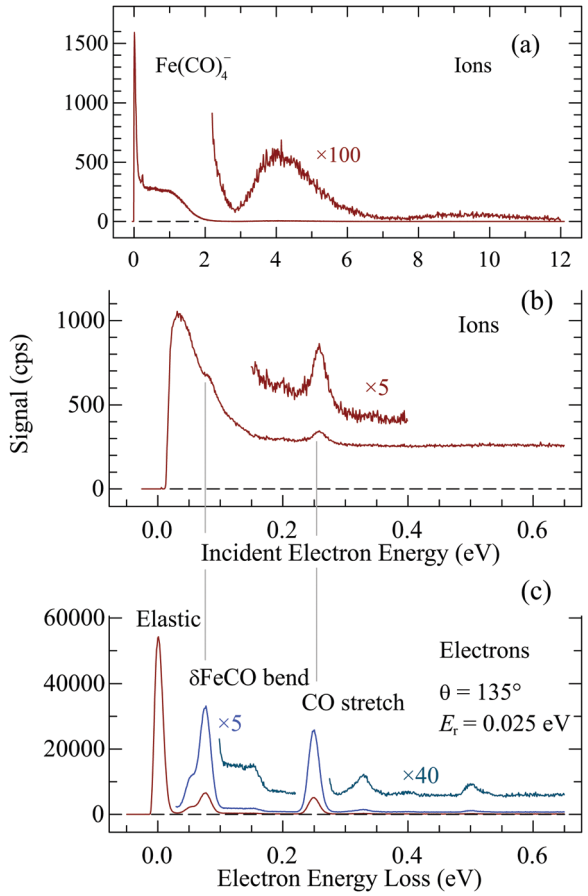

Fig. 1 (a) Yield of negative ions from gas-phase $Fe(CO)_5$, recorded on the spectrometer with hemispherical analyzers. The instrument measures total ion yield; the assignment of the low-energy signal to $Fe(CO)_4^-$ is deduced from Fig. 2. The ion kinetic energy analyzer was set to detect ions with E_{ion} = 0.025 eV. (b) The same spectrum on an expanded scale. (c) Yield of scattered electrons with a constant residual energy E_r = 0.025 eV, *i.e.*, the electron energy loss spectrum of $Fe(CO)_5$ in the energy range revealing vibrational excitation.

reveals that there is one narrow feature, key to the present discussion, and it corresponds to the C≡O stretch vibration. This indicates that the physics of the process is dominated by this vibration and justifies a one-dimensional treatment along the lines used successfully previously for the SF_6 molecule. (The situation is slightly complicated by the fact that $Fe(CO)_5$ has four CO-stretch vibrations with different symmetries,[29,30] with frequencies between 0.250 and 0.263 eV—too close to each other to be resolved in our experiment. But theoretical arguments indicate that it is the totally symmetrical mode which is mostly coupled to *s*-wave scattering.)

The multichannel effective range theory (ERT) is based on the matching equation[26]

$$\frac{d\psi}{dr} = f\psi, \quad (1)$$

where ψ is the external wavefunction taken at a radial distance r_0 from the origin and $f(s)$ is the logarithmic derivative of the internal wavefunction at the same distance.

We rewrite this equation in the representation of the eigenstate of the vibrational Hamiltonian for the CO stretch motion $H_0 = T(s) + V(s)$, where s is a normal stretch coordinate. Following Gauyacq and Herzenberg[27] we will now expand $f(s)$ in powers of s and assume the linear approximation

$$f = f_0 + f_1 s, \quad (2)$$

where f_0 and f_1 are complex parameters which generally depend on the electron energy. In the first order approximation of ERT, we neglect this dependence and consider them as complex constants. The imaginary part of f incorporates, in a phenomenological way, the loss of electron flux due to the IVR process. The energy dependence of the cross sections is taken care of by the external wave functions ψ, and this dependence can be very significant at low energies because of the long-range electron–molecule interaction.

Using the harmonic oscillator approximation, we obtain the matrix of logarithmic derivatives in the form

$$f_{v'v} = f_0\delta_{vv'} + \frac{f_1}{\sqrt{2\omega}}\left[\sqrt{v}\delta_{v'v-1} + \sqrt{v+1}\delta_{v'v+1}\right],$$

where ω is the frequency for the CO stretch vibrations. The matrix of the outside solutions can be written as

$$\psi = \psi^- - \psi^+ S$$

where $\psi^\pm$ are matrices of the outgoing and ingoing solutions and S is the scattering matrix. The matching equation is solved for S from which we obtain elastic, vibrational excitation and reaction cross sections. The complex parameters f_0, f_1 are unknown. For electron attachment to SF_6 they were determined empirically[26] by fitting to measured attachment and total cross sections. In the present case this information is absent, and we varied these parameters in a broad range to get an idea about the sensitivity of the negative-ion yield to these parameters. The known isotropic polarizability of the iron carbonyl, α = 189 a.u., was used to calculate the set of functions $\psi^\pm$ in different vibrational channels.

3.2 Electronically excited states of $Fe(CO)_5$

In order to provide insight into the nature of electronically excited states, we have calculated their energies and oscillator strengths (for dipole-allowed transitions). All the calculations have been carried out using the Amsterdam Density Functional program package, ADF2013.01.[31–33] An all electron quadruple ζ Slater-type orbital basis set augmented by four sets of polarization functions (QZ4P) has been used for all atoms. Symmetry constrained geometry optimization in the D_{3h} point group was performed using general gradient approximation consisting of Becke's exchange[34] and Perdew's correlation,[35,36] *i.e.* BP86 functional, with Becke's integration grid of good quality.[37,38] Vertical excitation energies and the corresponding oscillator strengths were calculated with the Time-Dependent DFT (TD-DFT) formalism, as implemented in ADF[39] at the same level of theory (BP86/QZ4P).

4 Results and discussion

4.1 DEA: experiment below 0.5 eV

Fig. 1 shows the negative ion yield from $Fe(CO)_5$ recorded on the electron spectrometer with hemispherical analyzers and Fig. 2 the mass-resolved ion yields for individual anions recorded on the setup with a trochoidal monochromator and a quadrupole mass filter. The spectra from the two instruments are in very good agreement. The ion yield shows an intense narrow peak at low energies. The results from the quadrupole instrument in Fig. 2 show that it is entirely due to the $Fe(CO)_4^-$ fragment. Fig. 1b shows that the peak is only about 70 meV wide. It thus appears to be less high in the spectra from the quadrupole instrument in Fig. 2, where it is convoluted with the 200 meV wide energy profile of the electron beam.

Essential features of the spectra agree with the early measurements of Compton and Stockdale,[8] except that their spectra did not show the 0 eV peak, but only a broad $Fe(CO)_4^-$ band with a maximum around 0.8 eV. The absence of the low energy peak in their spectrum can presumably be attributed to the failure of their instrument to generate sufficiently slow electrons. The present strong DEA signal close to 0 eV is consistent with the high electron attachment rates measured in an ICR cell[10] and by the flowing afterglow technique.[11]

The high resolution spectrum in Fig. 1b reveals previously unreported fine features: a cusp at 0.08 eV and a small peak at 0.26 eV. These structures closely resemble the structures close to thresholds for vibrational excitation that were observed, for example, in the DEA spectra of hydrogen halides or methyl halides.[25] Such structures are due to interchannel coupling—opening of the vibrational excitation channel reduces the flux into the DEA channel. Which vibrational levels of $Fe(CO)_5$ are excited at threshold is revealed by the electron-energy loss spectrum in Fig. 1c. Comparison of parts (b) and (c) of Fig. 1 reveals that the structures in the DEA cross section are very close to the thresholds for vibrational excitation. The two most prominent inelastic peaks in this spectrum correspond to excitation of δFeCO bending (overlap of ν_7,a_2'' and ν_{11},e' modes) and CO stretch (overlap of four normal modes involving CO stretch). (The mode numbering and assignment are identical to those of ref. 29 and 30.) This type of structures have been successfully reproduced by either the nonlocal resonance model or the effective range theory, and theory has always provided a very valuable insight into the mechanism of process.[25] We have applied the latter theory here, as detailed in the next subsection.

Revealing information about energy partitioning in the fragmentation process is provided by the ion kinetic energy distributions and we therefore measured ion kinetic energy spectra using the electrostatic instrument as shown in Fig. 3. The spectra are corrected for the analyzer response function, using the response function determined for electrons. Two distributions were measured. One, discussed in this section, at essentially zero incident electron energy, at the zero electron-volt DEA peak, and the other, discussed in a later section, at E_i = 1 eV, within the 1 eV resonance. Both are narrow; the widths at half height are 60 meV at E_i = 0.02 eV and 50 meV at E_i = 1.0 eV. Both distributions peak at the very low energy of 0.025 eV, whereby the instrumental ion collection efficiency drops below about 25 meV, so that the true distribution may peak at an even lower energy.

The maximum $Fe(CO)_4^-$ kinetic energy is given by the available excess energy E_e = EA − BDE + E_i, where EA is the electron affinity of the product negative ion $Fe(CO)_4^-$, BDE the $Fe(CO)_4$–CO bond dissociation energy, and E_i the incident electron energy. EA and BDE are, unfortunately, not known with high precision as discussed by Lacko *et al.*,[12] Shuman *et al.*[11] and Buathong *et al.*[14] Excess energy E_e = 0.6 ± 0.3 eV is obtained with EA = 2.4 ± 0.3 eV[20] and the experimental value of BDE = 1.8 ± 0.09 eV.[40] Taking the calculated value of BDE = 1.43 eV[12] yields E_e = 1.03 ± 0.3. E_i = 0.025 eV can be neglected in view of the large error bar of EA.

Only 14% of the total kinetic energy release is given to the $Fe(CO)_4^-$ fragment, so that the $Fe(CO)_4^-$ maximum kinetic energy is 0.09 ± 0.04 eV or 0.15 ± 0.04 eV for the two choices of BDE, respectively.

These numbers are higher than the measured peak position of 0.025 eV (Fig. 3). This indicates that a major fraction of the available excess energy is left as vibrational energy of the $Fe(CO)_4^-$ fragment and thus supports the hypothesis of substantial IVR in

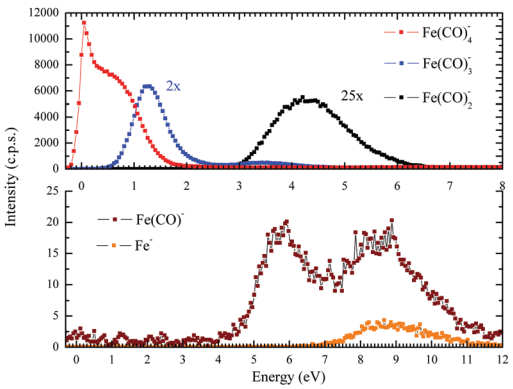

Fig. 2 Negative ion yield as a function of electron energy recorded on the DEA spectrometer with a trochoidal monochromator and a quadrupole mass filter.

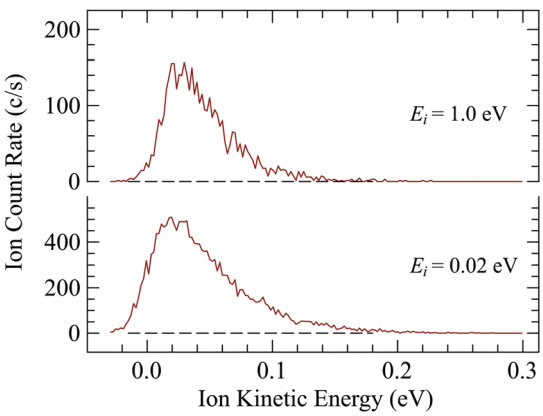

Fig. 3 Ion kinetic energy distributions recorded at the two incident electron energies indicated.

the $Fe(CO)_5^-$ attachment complex. On the other hand, the fact that the tail of the distribution extends up to about 0.15 eV for E_i = 0.025 eV in Fig. 3, that is, that it extends to an energy higher than thermal, indicates that the IVR process is not complete, that the $Fe(CO)_4^-$ fragment is not fully thermalized. This result agrees with the conclusion of Buathong *et al.*,[14] based on the study of electron attachment in Rydberg atom collisions, that partial but not complete statistical redistribution of the excess energy prior to dissociation occurs, indicating dissociation of $Fe(CO)_5^-$ on time scales of a few vibrational periods.

Finally, since virtual states, implied in the theoretical treatment below, are manifested by a sharp rise of the elastic cross section at low energies, we report the elastic cross section in Fig. 4. The cross section does rise very sharply at low energy (observe that it is shown on a log–log scale), providing experimental evidence for a virtual state. A pronounced Ramsauer–Townsend minimum occurs at 0.28 eV.

4.2 DEA: theory below 0.5 eV

Our first choice of the ERT parameters was motivated by our previous calculations of electron attachment to SF_6.[26] Specifically, we have chosen r_0 = 3.23, f_0 = 0.989 + 0.108i, f_1 = −0.00991 + 0.0025i. (All parameters are in a.u.) Although what can be called the "size" of $Fe(CO)_5$ is greater than r_0, the ERT radius cannot be taken too large as this leads to the energy dependence of the parameters f_0 and f_1. Therefore we consider the extension of the polarization potential into the region $r_0 < r < R$ (where R is the effective size of the molecule) as an empirical way to incorporate the electron–molecule interaction in this region. Since the Fe–C distance is 1.81 Å and the C–O distance is 1.15 Å,[29,30] R should be about 6 a.u.

The listed set of parameters leads to a virtual-state scattering at low energies, similar to e–SF_6 scattering. Variation of f_0 and f_1 resulted in the following observations: the increase of $\mathrm{Re}\,f_0$ leads to a less pronounced virtual-state effect. The $\mathrm{Im}\,f_0$ parameter mostly controls coupling between the scattering and attachment channels, and therefore influences only the magnitude of the attachment cross section, but not its shape. The parameter $\mathrm{Re}\,f_1$ influences less the attachment cross section as it is mostly responsible for vibrational excitation. Finally, the attachment cross section has very little sensitivity to $\mathrm{Im}\,f_1$.

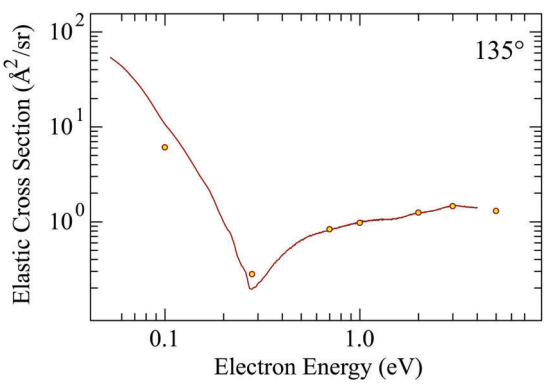

Fig. 4 Differential elastic cross section measured at θ = 135°.

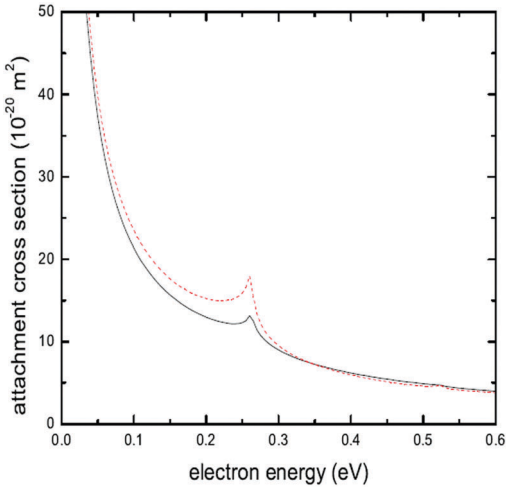

Fig. 5 Electron attachment to iron pentacarbonyl calculated with two sets of parameters as described in the text. Solid (black curve), $\mathrm{Re}\,f_1$ = −0.0991; dashed (red) curve, $\mathrm{Re}\,f_1$ = −0.143.

In Fig. 5 we present two curves for attachment cross sections corresponding to the original choice of parameters and with $\mathrm{Re}\,f_1$ replaced by −0.143. The cusp at the CO stretch threshold is caused by the virtual state due to the e–$Fe(CO)_5$ polarization attraction. It is well known[26,41] that by increasing e–M attraction, one can convert the virtual-state cusp into vibrational Feshbach resonance. In Fig. 6 we show the result of this numerical experiment performed by increasing the polarizability α. At α = 220 a.u. the cusp becomes very pronounced meaning that the virtual state is on the brink of conversion to the bound state. Then at α = 230 a.u., a below-threshold resonance appears meaning that the virtual state has been converted into a bound state.

The magnitude of the cross section can be checked by calculation of the attachment rate coefficient k and comparison with the measurements of Shuman *et al.*,[11] who obtained

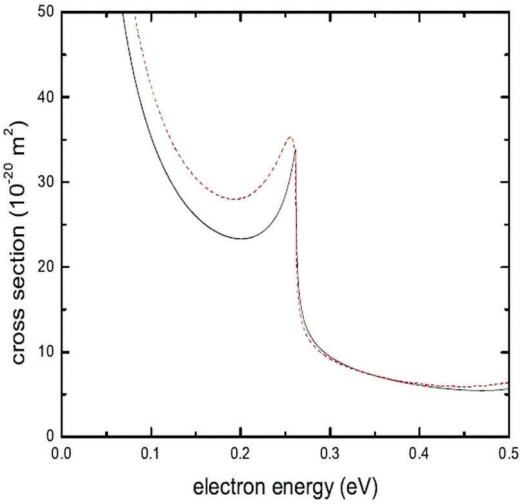

Fig. 6 Electron attachment to iron pentacarbonyl calculated with polarizabilities α = 220 a.u. (solid black curve) and α = 230 a.u. (dashed red curve).

$k = (7.9 \pm 1.4) \times 10^{-8}$ cm^3 s^{-1} at $T = 300$ K and $k = (8.8 \pm 2) \times 10^{-8}$ cm^3 s^{-1} at $T = 400$ K. Our first choice of the parameter Ref_1 (solid curve in Fig. 5) gives $k = 5.92 \times 10^{-8}$ cm^3 s^{-1} and the second choice (dashed curve in Fig. 5) $k = 6.26 \times 10^{-8}$ cm^3 s^{-1} at $T = 300$ K. As mentioned, the absolute value of the cross section is more sensitive to the parameter Ref_0. In particular, the choice Re$f_0 = 0.7$ a.u. leads to $k = 8.14 \times 10^{-8}$ cm^3 s^{-1} at $T = 300$ K, closer to the experimental value. With regard to the temperature dependence, since the theory incorporates explicitly only C–O stretch vibrations, the cross section is almost independent of vibrational temperature at thermal energies, and all temperature dependence is determined by the electron energy dependence of the cross section. In particular, with the choice Re$f_0 = 0.7$ a.u., the rate coefficient drops from 8.14×10^{-8} to 7.45×10^{-8} cm^3 s^{-1}. Although this drop is within the experimental uncertainty, it could be possible that the actual rate coefficient grows with the temperature because of the growth of population of excited states corresponding to other modes with lower frequencies not included in our model.

Finally we add that the attachment rate, although rather high, is small as compared to the prediction of the Vogt–Wannier model[42] describing quantum capture by the polarization potential. The Vogt–Wannier thermal rate coefficient is given by[43]

$$k_{VW} = 7.755 \times 10^{-8}\alpha^{1/2} \text{ cm}^3 \text{ s}^{-1}$$

where α is taken in a.u. For iron pentacarbonyl this estimate exceeds the actual value by a factor of 13.5. This makes this molecule a rather inefficient attacher[11] as compared, for example, with SF_6 and CCl_4.

4.3 DEA: experiment above 0.5 eV

This section discusses the DEA bands above 0.5 eV, shown in Fig. 1 and 2. Our spectrum is in excellent agreement with that of Schukin *et al.*[9] A number of resonant bands appear and we attempt their assignment to shape and Feshbach resonances. Independent information about shape resonances is obtained from the cross sections for vibrational excitation (VE) shown in Fig. 7. All VE cross sections have very intense threshold peaks which are due to the virtual state discussed in Section 4.2. A number of broad bands can be discerned at higher energies, assigned as overlapping shape resonances with temporary occupation of CO-located virtual orbitals in $Fe(CO)_5$ resulting from overlapping π_{CO}* orbitals.

The $v = 0 \rightarrow 1$ VE cross section of carbon monoxide is also shown in Fig. 7 for comparison and shows that the $Fe(CO)_5$ π* bands are in the right energy range.

There is only a limited correspondence between the DEA and the VE spectra. The 1.2 eV $Fe(CO)_3^-$ band in Fig. 2 corresponds to the 1.3 eV band in the CO stretch excitation cross section ($\Delta E = 0.252$ eV) in Fig. 7. The 0.7 eV $Fe(CO)_4^-$ band in Fig. 2 does not have any clear corresponding band in the VE spectra. It could be that there is a π* resonance at 0.7 eV but is obscured by the tail of the threshold peaks in the VE spectra. It could also be that the 0.7 eV $Fe(CO)_4^-$ band in the DEA spectra is caused by the same π* resonance as the 1.3 eV band in the VE spectra,

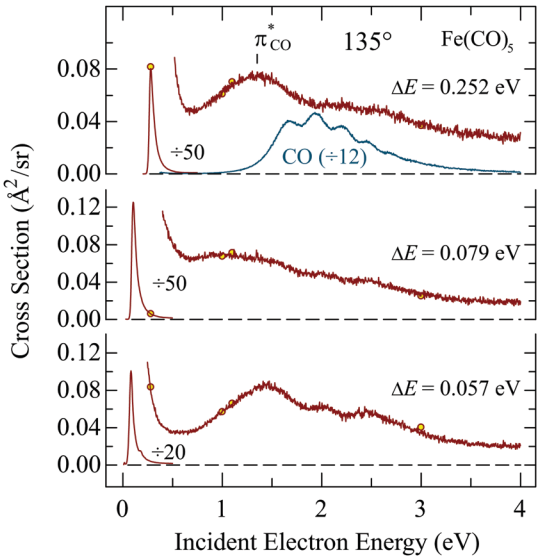

Fig. 7 Cross sections for vibrational excitation, indicative of resonances.

but the DEA band is lowered by the "kinetic shift", *i.e.*, the resonance width being narrower at lower energies.

Electronic Feshbach resonances are generally located 0–0.4 eV below their parent triplet electronically excited state and should thus follow a pattern similar to that of triplet bands in an electron energy loss (EEL) spectrum (shown in Section 4.5). Comparison of the EELS spectrum with the DEA spectrum in Fig. 2 reveals such a similarity; in particular the shapes of the 5.9 and 8.8 eV $Fe(CO)^-$ bands in Fig. 2 are reminiscent of the 5.76 eV and 9.2 eV triplet bands in the EEL spectrum, permitting the assignment of these DEA bands to Feshbach resonances.

Finally we address the question of the decay dynamics of the higher-lying resonances, in particular the one which gives rise to the 1 eV shoulder in the ion yield in Fig. 1. We do this by recording the spectrum of electrons detached following the capture of a 1 eV electron, as shown by the center trace in Fig. 8. The excitation of the CO stretch vibration and that an overtone of it is excited are indications of a temporary occupation of a π_{CO}* orbital. The interesting feature is the group of electrons around the energy-loss of 1 eV in the center spectrum of Fig. 8, *i.e.*, electrons detached with nearly zero energy. Such electrons are a manifestation of an extremely fast radiationless decay, fast enough to compete with the ns-ps fast autodetachment of the resonance. This process, presumably mediated by a conical intersection between the potential surfaces of the 1 eV π_{CO}* shape resonance and the ground state $Fe(CO)_5^-$, leads to a rapid conversion of electronic to vibrational energy followed by detachment of thermal electrons.

Note the unusual situation in the $E_i = 0.28$ eV spectrum at the bottom of Fig. 8, where, as a consequence of the threshold peak in the CO stretch excitation (see the top trace in Fig. 7) and of the Ramsauer–Townsend minimum in the elastic cross section (Fig. 4), the elastic peak is nearly 20× lower than the inelastic peak at $\Delta E = 0.252$ eV!

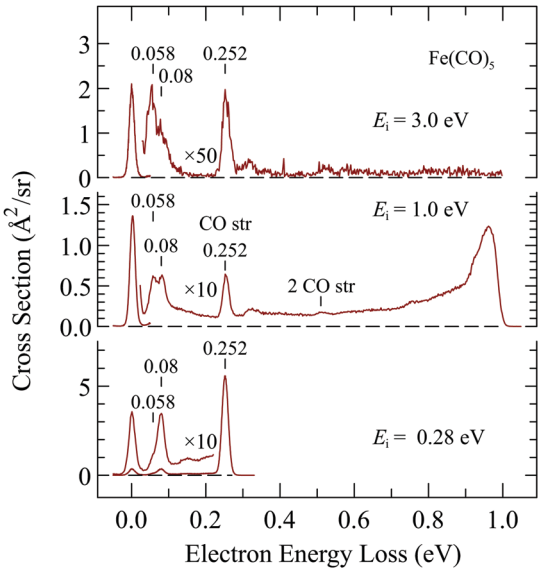

Fig. 8 Distributions of scattered electron energies at the incident energies of 0.28, 1.0 and 3.0 eV.

4.4 Two-dimensional EEL spectrum

Two-dimensional (2D) spectra provide insight into the dynamics of resonances by mapping their decay channels and their capacity to thermalize electrons.[44–46] The 2D spectrum of $Fe(CO)_5$ is shown in Fig. 9.

Features already discussed above can be recognized: (i) the Ramsauer–Townsend minimum can be discerned at incident energy E_i = 0.28 eV on the 'elastic ridge' (situated vertically at an energy-loss ΔE = 0), (ii) the threshold peaks in the excitation of individual vibrational modes, and (iii) enhancement of the excitation of the δFeCO bend and CO stretch vibrations in the 0.8–1.6 eV incident energy range, indicative of π^* resonances.

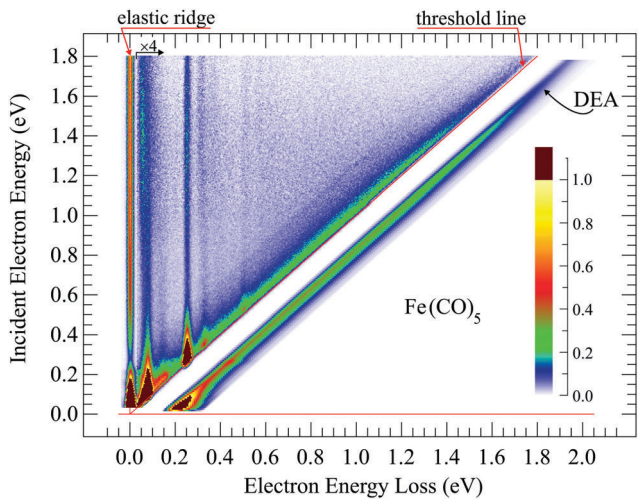

Fig. 9 Two-dimensional electron energy loss spectrum and DEA spectrum. The incident electron energy scale (the ordinate) refers to both the 2D energy loss spectrum and the DEA spectrum. The energy loss scale applies to the 2D spectrum only; it does not apply to the DEA spectrum—the horizontal scale shows the ion kinetic energy there.

Note that ejection of thermal electrons is mapped along the diagonal "threshold line" where $\Delta E = E_i$, *i.e.*, E_r = 0. Thus the "threshold ridge" signal (green diagonal line in Fig. 9) is interesting—it reveals efficient ejection of thermal electrons in the incident energy range of 0 to ~1.4 eV. It is indicative of the fast dynamics and rapid thermalization of the electrons by IVR, followed by thermal detachment. Further interesting is that the DEA signal, also shown for comparison in the same figure, mimics the shape of the yield of thermal electrons. This indicates that the two processes are closely related—attachment of an electron into a π^* resonance is followed by very rapid IVR leading to a hot $Fe(CO)_5^-$ anion which decays by one of the two competing decay processes, detachment of a thermal electron or a thermal loss of a CO ligand.

There is a subtle interesting feature in the 2D spectrum: a faint diagonal line parallel to the 'threshold ridge', but shifted left. It indicates enhanced ejection of electrons with a discrete energy E_r = 0.250 eV, independent of the incident energy, and over the same range of incident energies where the zero eV electrons are also ejected. With a certain overstatement one could say that the collision complex has become an electron monochromator—electrons with a range of energies are attached and monoenergetic electrons are ejected. A plausible explanation is that the thermalized $Fe(CO)_5^-$ can, apart from ejecting a thermal, nearly 0 eV electron, also eject a 0.250 eV electron by simultaneously losing one quantum of the CO stretch vibration. The CO stretch mode promotes detachment. The process where a specific vibrational mode promotes electron detachment has also been observed in acrylonitrile.[44,46] Autodetachment mediated by specific vibrational modes has also been reported by Verlet and coworkers in a time-resolved photodetachment study of the *para*-toluquinone trimer cluster anion.[47]

4.5 Electronic excitation

Fig. 10 shows the electron-energy loss spectra in the energy range 2–15 eV, measured on the spectrometer with hemispherical analyzers. The spectra were recorded at 0° and 180° scattering angles. In order to keep the analyzer response function constant, the spectra were recorded at the constant residual energy of an electron E_r and the incident energy was scanned (the *x*-axis corresponds to the energy loss, a difference between the incident and residual energy).

It is well established[48] that if the incident electron has high energy and undergoes little deflection (large impact parameters), the long-range interaction with the molecule leads to selection rules identical to those for optical transitions. On the other hand, spin-forbidden transitions, due to spin-exchange scattering, are preferred at low electron energies (incident electron wavelength comparable with the wavelength of valence electrons) and have nearly isotropic angular distribution. The excitation of dipole-allowed singlet states thus dominates in the forward direction at higher energies and the excitation of triplet states is favored at low electron energies and large scattering angles. In Fig. 10a we thus show present TD-DFT excitation energies and oscillator strengths for dipole-allowed transitions. In Fig. 10b we compare the backward EELS spectrum with the

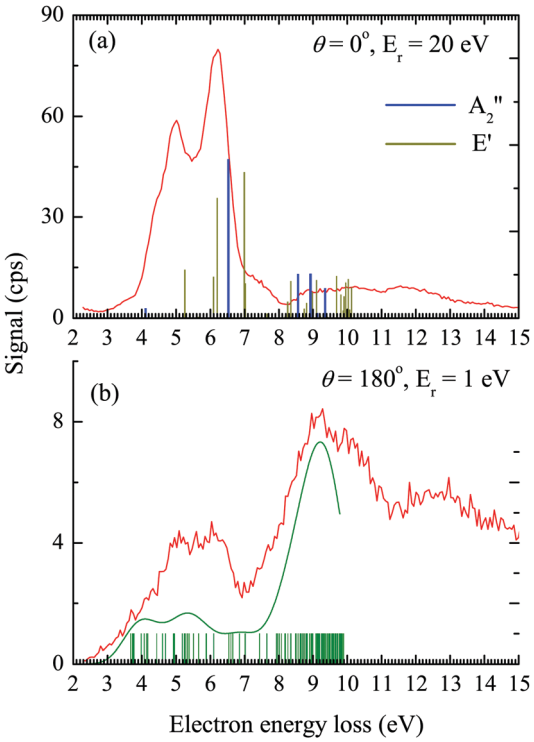

Fig. 10 Electron-energy loss spectra of gas phase $Fe(CO)_5$ recorded under two different scattering conditions. Vertical bars are at the calculated (TD-DFT) positions of the excited states; in panel (a) their heights correspond to oscillator strengths. Panel (a) shows the singlet states of E′ and A_2'' symmetries, and panel (b) the triplet states.

calculated excitation energies of triplet states. Since the individual bars at the calculated positions of triplet states are not discernible, we have convoluted the calculated spectrum with a Gaussian of 1 eV FWHM. The tables with energies, configurations and (for allowed transitions) oscillator strengths are presented in the ESI.†

$Fe(CO)_5$ is a low-spin d^8 complex with a trigonal bipyramidal structure. In the D_{3h} point group iron d orbitals split into e′ (d_{xy}, $d_{x^2-y^2}$), e″ (d_{xz}, d_{yz}) and a_1' (d_{z^2}) that combine with the suitable MOs of CO ligands. As a consequence, the five highest occupied and the five lowest unoccupied MOs of $Fe(CO)_5$ involve iron d orbitals.[49] MOs with dominant metal d-orbital character are strongly σ-antibonding, empty $14a_1'$, and the highest occupied 10e′ and 3e″. The latter two sets are the result of the π-back-bonding of the iron orbitals with the π* carbonyl orbitals. The ground electronic state of $Fe(CO)_5$ is $^1A_1'$ and dipole-allowed transitions are to the excited E′ and A_2'' states, shown in Fig. 10 as olive-green and blue bars, respectively. The calculated excitation energies and oscillator strengths are in excellent agreement with the EELS spectrum (Fig. 10a) and with near-UV gas-phase[50] and solution spectra.[51] In particular, the most prominent bands at 5.0 and 6.3 eV can be clearly assigned as metal-to-ligand charge transfer (MLCT) transitions to the E′ and A_2'' excited states, respectively. Excitation energies by TDDFT are overestimated by ~0.25 eV. Recent high-level *ab initio* studies[52,53] reported significant overestimation of the first band (by 0.6–1.5 eV). The maximum in the TDDFT spectrum lies between two groups of E′ states with considerable oscillator strengths. The first group is of mixed MLCT and Rydberg 3d → 4s character, while the second one is of MLCT and Rydberg 3d → 4p type. In addition, our TDDFT results explain all the other experimental features. The gradual ascent of the signal in the range 4–5 eV is dominated by MLCT transitions (one A_2'' and two E′ states). A dipole-allowed E′ d–d transition is also predicted to be in this range, although it carries little oscillator strength. Finally, the broad band at energies higher than 8 eV is seen to be a consequence of a group of high-lying ligand-to-metal charge transfer and intra-ligand transitions.

Very good agreement is also obtained for singlet–triplet transitions (Fig. 10b). Obviously, the peaks in the EELS spectrum correspond to the regions where a high density of triplet states is calculated by TDDFT. The lowest triplet, $^3E'$ state, due to the d–d spin–flip transition ($10e' \rightarrow 14a_1'$) is calculated to be 0.56 eV lower than the corresponding singlet state. It is noteworthy to mention that one component of this degenerate state becomes the ground electronic state upon dissociation of one CO ligand.[54,55]

5 Conclusions

We provide new insight into elementary electron-induced decomposition processes in gas phase $Fe(CO)_5$.

The dominant feature in DEA is a high and narrow (70 meV) peak in the $Fe(CO)_4^-$ formation (cleavage of one metal–ligand bond) at near-zero incident electron energy. Fine structures are observed on the tail of this peak, at vibrational excitation thresholds.

A model based on the effective range theory with complex boundary conditions reproduces these structures and interprets them as evidence of virtual state scattering, with an important role being played by intramolecular vibrational redistribution (IVR).

The hypothesis of a virtual state dominating low energy (<0.5 eV) processes receives further support from the observation of threshold peaks in vibrational excitation cross sections and from a dramatic rise of the elastic cross section at very low energies.

The second highest DEA feature is a $Fe(CO)_4^-$ peak around 0.8 eV which we interpret as due to a π* resonance. A two-dimensional (2D) EEL spectrum reveals efficient detachment of nearly zero eV electrons over the same range of incident electron energies as this DEA band, *i.e.*, the capacity of $Fe(CO)_5$ to thermalize electrons within this π* resonance. This is taken as experimental evidence for a rapid IVR process being important also for this π* resonance—it converts the anion formed by the initial attachment into a hot $Fe(CO)_5^-$ anion that then decays either by loss of one CO ligand or by detachment of a thermal electron. The low measured kinetic energies of the $Fe(CO)_4^-$ fragment provide additional evidence for IVR taking place prior to dissociation.

The 2D spectrum also reveals a somewhat exotic capacity of the CO stretch vibrational mode to promote detachment in the hot $Fe(CO)_5^-$ anion, leading to a small yield of superthermal

electrons with a discrete energy equal to the CO stretch vibrational quantum. These electrons are observed over a range of incident electron energies covering the entire width of the π^* resonance.

Combination of electron-energy loss spectra and TD-DFT calculations characterizes the electronically excited states of $Fe(CO)_5$. The calculations agree with the experiment very well and reproduce both the spin-allowed and spin-forbidden transitions. The significance of these results is that (i) these excited states represent a path to neutral dissociation and (ii) the energies of the triplet states provide indication of energies of Feshbach resonances and permit conclusions about assignments of the higher-lying DEA bands.

The importance of the present findings is that they reveal mechanisms *via* which iron pentacarbonyl is dissociated at various energy ranges. The electrons with energies below 1 eV lead to very efficient DEA. The DEA cross section is strongly enhanced by the long-range forces: the high polarizability of $Fe(CO)_5$ leads to a virtual state scattering. The presence of this virtual state leads to a high DEA cross section. The long-range forces are thus crucial for the low-energy DEA. On the other hand, the electronic excitation, the first step in the neutral dissociation pathway, can be viewed as direct excitation and thus a short range process. This difference opens a major question: when the iron pentacarbonyl reacts with electrons in an environment (*e.g.*, adsorbed at a surface under realistic FEBID conditions), the typical distances between molecules (or $Fe(CO)_5$ molecules and 'bulk') are smaller than the distances on which the electron-induced-dipole interaction is operative. How does this fact influence the low-energy DEA effectivity? This question has been addressed in our cluster beam study.[56]

Conflicts of interest

There are no conflicts to declare.

Acknowledgements

This work has been supported by the Czech Science Foundation project No. 17-04844S (J. F.), Swiss National Science Foundation Project No. 200020-144367/1 (M. A.), US National Science Foundation Grant No. PHY-1401788 (I. I. F), Serbian Ministry of Science Project 172035 (M. Z.), and by several short-term scientific missions within the COST Action CM1301 CELINA. P. P. and M. Š. acknowledge support from the Slovak Grant Agency VEGA 1/0733/17, Slovak Research and Development Agency project APVV-15-0580, and EU's Horizon 2020 program under grant agreement No. 692335.

References

1 I. Utke, P. Hoffmann and J. Melngailis, *J. Vac. Sci. Technol., B*, 2008, **26**, 1197.
2 M. Takeguchi, M. Shimojo and K. Furuya, *Nanotechnology*, 2005, **16**, 1321–1325.
3 T. Lukasczyk, M. Schirmer, H.-P. Steinrück and H. Marbach, *Small*, 2008, **4**, 841–846.
4 J. M. De Teresa and A. Fernández-Pacheco, *Appl. Phys. A: Mater. Sci. Process.*, 2014, **117**, 1645.
5 R. M. Thorman, T. P. R. Kumar, D. H. Fairbrother and O. Ingólfsson, *Beilstein J. Nanotechnol.*, 2015, **6**, 1904–1926.
6 H. Miyazoe, I. Utke, H. Kikuchi, S. Kiriu, V. Friedli, J. Michler and K. Terashima, *J. Vac. Sci. Technol., B: Nanotechnol. Microelectron.: Mater., Process., Meas., Phenom.*, 2010, **28**, 744.
7 B. Geier, C. Gspan, R. Winkler, R. Schmied, J. D. Fowlkes, H. Fitzek, S. Rauch, J. Rattenberger, P. D. Rack and H. Plank, *J. Phys. Chem. C*, 2014, **118**, 14009.
8 R. N. Compton and J. A. D. Stockdale, *Int. J. Mass Spectrom. Ion Phys.*, 1976, **22**, 47–55.
9 P. V. Shchukin, M. V. Muftakhov and R. V. Khatymov, *Issled. Russ.*, 2005, 1672.
10 P. M. George and J. L. Beauchamp, *J. Chem. Phys.*, 1982, **76**, 2959.
11 N. S. Shuman, T. M. Miller, J. F. Friedman and A. A. Viggiano, *J. Phys. Chem. A*, 2012, **117**, 1102.
12 M. Lacko, P. Papp, K. Wnorowski and Š. Matejčík, *Eur. Phys. J. D*, 2015, **69**, 84.
13 M. Lacko, P. Papp, Š. Matejčík and K. Wnorowski, *WDS'14 Proceedings of Contributed Papers – Physics*, 2014, pp. 292–297.
14 S. Buathong, M. Kelley and F. B. Dunning, *J. Chem. Phys.*, 2016, **145**, 134309.
15 S. Massey, A. D. Bass, E. Alizadeh and L. Sanche, *J. Phys.: Conf. Ser.*, 2015, **635**, 062012.
16 S. Massey, A. D. Bass and L. Sanche, *J. Phys. Chem. C*, 2015, **119**, 12708.
17 C. Hauchard and P. A. Rowntree, *Can. J. Chem.*, 2011, **89**, 1163–1173.
18 J. Lengyel, J. Kočišek, M. Fárník and J. Fedor, *J. Phys. Chem. C*, 2016, **120**, 7397–7402.
19 J. Lengyel, J. Fedor and M. Fárník, *J. Phys. Chem. C*, 2016, **120**, 17810–17816.
20 P. C. Engelking and W. C. Lineberger, *J. Am. Chem. Soc.*, 1979, **101**, 5569.
21 M. Zlatar, M. Allan and J. Fedor, *J. Phys. Chem. C*, 2016, **120**, 10667–10674.
22 M. Allan, *J. Phys. B: At. Mol. Phys.*, 1992, **25**, 1559.
23 M. Allan, *J. Phys. B: At. Mol. Phys.*, 2005, **38**, 3655.
24 M. Stano, Š. Matejčík, J. D. Skalny and T. D. Märk, *J. Phys. B: At. Mol. Phys.*, 2003, **36**, 261.
25 H. Hotop, M.-W. Ruf, M. Allan and I. I. Fabrikant, *Adv. At., Mol., Opt. Phys.*, 2003, **49**, 85.
26 I. I. Fabrikant, H. Hotop and M. Allan, *Phys. Rev. A: At., Mol., Opt. Phys.*, 2005, **71**, 022712.
27 J. P. Gauyacq and A. Herzenberg, *J. Phys. B: At. Mol. Phys.*, 1984, **17**, 1155.
28 L. D. Landau and E. M. Lifshitz, *Quantum Mechanics (Non-relativistic Theory)*, Butterworth-Heinenann, 1981.
29 V. Jonas and W. Thiel, *J. Chem. Phys.*, 1995, **102**, 8474–8484.
30 J. H. Jang, J. G. Lee, H. Lee, Y. Xie and H. F. Schaefer III, *J. Phys. Chem. A*, 1998, **102**, 5298–5304.

31 C. Fonseca Guerra, J. G. Snijders, G. te Velde and E. J. Baerends, *Theor. Chem. Acc.*, 1998, **99**, 391–403.
32 G. te Velde, F. M. Bickelhaupt, E. J. Baerends, C. Fonseca Guerra, S. J. A. van Gisbergen, J. G. Snijders and T. Ziegler, *J. Comput. Chem.*, 2001, **22**, 931–967.
33 ADF: Density Functional Theory (DFT) software for chemists, version 2013.01, http://www.scm.com/, 2013.
34 A. D. Becke, *Phys. Rev. A: At., Mol., Opt. Phys.*, 1988, **38**, 3098–3100.
35 J. P. Perdew, *Phys. Rev. B: Condens. Matter Mater. Phys.*, 1986, **33**, 8822–8824.
36 J. P. Perdew, *Phys. Rev. B: Condens. Matter Mater. Phys.*, 1986, **34**, 7406.
37 A. D. Becke, *J. Chem. Phys.*, 1988, **88**, 2547–2553.
38 M. Franchini, P. H. T. Philipsen and L. Visscher, *J. Comput. Chem.*, 2013, **34**, 1819–1827.
39 F. Kootstra, P. L. de Boeij and J. G. Snijders, *J. Chem. Phys.*, 2000, **112**, 6517–6531.
40 K. E. Lewis, D. M. Golden and G. P. Smith, *J. Am. Chem. Soc.*, 1984, **106**, 3905–3912.
41 E. Leber, I. I. Fabrikant, J. M. Weber, M.-W. Ruf and H. Hotop, in *Dissociative Recombination: Theory, experiment and applications IV*, ed. A. Mitchell and I. F. Schneider, World Scientific, Singapore, 2000, pp. 69–76.
42 E. Vogt and G. H. Wannier, *Phys. Rev.*, 1954, **95**, 1190–1198.
43 I. I. Fabrikant and H. Hotop, *Phys. Rev. A: At., Mol., Opt. Phys.*, 2001, **63**, 022706.
44 K. Regeta and M. Allan, *Phys. Rev. Lett.*, 2013, **110**, 203201.
45 K. Regeta and M. Allan, *J. Chem. Phys.*, 2015, **142**, 184307.
46 M. Allan, K. Regeta, J. D. Gorfinkiel, Z. Mašín, S. Grimme and C. Bannwarth, *Eur. Phys. J. D*, 2016, **70**, 123.
47 J. N. Bull and J. R. R. Verlet, *Sci. Adv.*, 2017, **3**, e1603106.
48 M. Allan, *J. Electron Spectrosc. Relat. Phenom.*, 1989, **48**, 219–351.
49 A. J. Atkins, M. Bauer and C. R. Jacob, *Phys. Chem. Chem. Phys.*, 2015, **17**, 13937–13948.
50 M. Kotzian, N. Roesch, H. Schroeder and M. C. Zerner, *J. Am. Chem. Soc.*, 1989, **111**, 7687–7696.
51 M. Dartiguenave, Y. Dartiguenave and H. B. Gray, *Bull. Soc. Chim. Fr.*, 1969, **12**, 4223.
52 L. M. J. Huntington and M. Nooijen, *J. Chem. Phys.*, 2015, **142**, 194111.
53 L. M. J. Huntington, O. Demel and M. Nooijen, *J. Chem. Theory Comput.*, 2016, **12**, 114–132.
54 M. Poliakoff and E. Weitz, *Acc. Chem. Res.*, 1987, **20**, 408–414.
55 M. Besora, J.-L. Carreón-Macedo, Á. Cimas and J. N. Harvey, *Adv. Inorg. Chem.*, 2009, **61**, 573–623.
56 J. Lengyel, P. Papp, Š. Matejčík, J. Kočišek, M. Fárník and J. Fedor, *Beilstein J. Nanotechnol.*, 2017, **8**, 2200.